Applied Geochemistry 123 (2020) 104774

Contents lists available at ScienceDirect

Applied Geochemistry

journal homepage: http://www.elsevier.com/locate/apgeochem

Insights on the effect of pyrite liberation degree upon the acid mine drainage potential of sulfide flotation tailings

Carolina Mafra [a], Hassan Bouzahzah [a,*], Lachezar Stamenov [b], Stoyan Gaydardzhiev [a]

[a] University of Liege, GeMMe - Minerals Engineering and Recycling, Sart-Tilman Campus-B52, 4000, Liège, Belgium
[b] Dundee Precious Metals Chelopech, 2087, Chelopech, Bulgaria

ARTICLE INFO

Editorial handling by Prof. M. Kersten

Keywords:
Mine tailings
Acid mine drainage
Mineral liberation
Automated mineralogy
Statistic test
Kinetic test

ABSTRACT

A new insight into the way in which the mineralogical composition and texture (liberation) of sulfides govern the geochemical behavior of the tailings in terms of acid mine drainage (AMD) generation is presented. Two samples were taken from Dundee Precious Metals Chelopech (DPM-Ch) tailings management facility (TMF). They were likewise subjected to flotation to recover reactive (liberated and partially liberated) pyrite whilst the unreacted (locked) pyrite was kept in the tailings fraction. Geochemical (static and kinetic) tests were performed on the collected samples and tailings after flotation. A scanning electron microscope based automated mineralogy system was used to characterize them in terms of modal mineralogy, liberation degree and particle size. The absolute acid-generating potential (AP) defined by the Sobek method most likely overestimates the effective AP when pyrite is locked into non–reactive gangue minerals. Hence, the locked pyrite may unfavorably lead to increased tailings management costs. Therefore, the automated mineralogy data was used to calculate the effective AP of the tailings taking into account pyrite grade and its liberation degree. Based on these findings, it could be assumed that the amount of lime required to neutralize the acidity produced by pyrite oxidation would be considerably reduced (in the studied case nearly 4 times) if environmental desulfurization by flotation is practiced and the liberation degree of the acid-producing minerals is taken into account.

1. Introduction

Acid rock drainage (ARD) constitutes an acidic runoff formed under natural phenomena when sulfide-bearing rocks are exposed to oxygen and moisture. Sulfide minerals are thermodynamically unstable under ambient conditions, which leads to oxidative weathering and release of H^+ to water (Lindsay et al., 2015). The fluid released in such conditions is characterized by low pH, high specific conductivity and enrichment in sulfate and dissolved elements (Broadhurst and Harrison, 2015). In this context, the exploitation of sulfide-bearing ores accelerates the ARD process due to the elevated exposure of the minerals. The phenomenon is then known as acid mine drainage (AMD) (Kleinmann et al., 1981; Lapakko, 1994; Blowes et al., 1994; Nicholson and Scharer, 1994; Perkin et al., 1995; Sherlock et al., 1995; Blowes et al., 2003; Parbhakar-Fox et al., 2009; Parbhakar-Fox and Lottermoser, 2015).

Static and kinetic tests are commonly used to assess the AMD potential of an unknown material. The static test, also called acid-base accounting (ABA), measures the balance between acid-generating potential (AP) and acid-neutralizing potential (NP) present in the material (Ferguson and Morin and Hutt, 1994; Miller et al., 1991). On the other hand, the kinetic test tries to mimic, at an accelerated rate, the oxidation of the targeted material like being placed at a mining site. This test also allows the quantification of evolution of water chemistry over time (Villeneuve et al., 2003). Although the kinetic test provides a more accurate prediction regarding the oxidation rate by resembling field conditions, the required analytical equipment is relatively expensive and the procedures are time consuming (Parbhakar-Fox et al., 2009). Therefore, a viable alternative in forecasting the AMD potential could be offered by the static test which is more rapid, relatively simple and needs less sophisticated instrumentation (Parbhakar-Fox et al., 2009).

The ABA test defines the Net Neutralization Potential (NNP) and the Neutralization Potential Ratio (NPR) of an unknown sample by comparing its AP and NP values (NNP=NP-AP and NPR=NP/AP). The AP and NP parameters are usually obtained through chemical and mineralogical methods. The first one uses geochemical data as proxies, whereas the mineralogical approach is based on calculated AP and NP through equations that take into account the mineralogical composition of the mining waste (Kwong, 1993; Lawrence and Scheske, 1997;

* Corresponding author.
E-mail addresses: hassan.bouzahzah@uqat.ca, h.bouzahzah@gmail.com (H. Bouzahzah).

https://doi.org/10.1016/j.apgeochem.2020.104774
Received 30 March 2020; Received in revised form 11 September 2020; Accepted 14 September 2020
Available online 18 September 2020
0883-2927/© 2020 Elsevier Ltd. All rights reserved.

Paktunc (1999); Bouzahzah et al., 2013; Chopard et al., 2015). However, neither protocol focuses on the genuine texture of the sample which in practice, plays an important role in the AMD generation (Parbhakar-Fox and Lottermoser, 2015; Elghali et al., 2018).

The traditional protocol to conduct an ABA test is the Sobek method. However, this protocol is notorious in generating biased results due to its capacity to overestimate the NP and AP (Bouzahzah et al., 2014, 2015). The two major limitations associated with the original Sobek test are: (1) increased reactivity of silicates and clay minerals due to the fact that the test is performed under high temperature, and (2), the Fe, Mn and Al, released by Fe–Mn-carbonates and Fe–Al-silicates dissolution, do not have time to complete hydrolysis and precipitate as hydroxides, contributing to the acid-generating potential instead of neutralizing potential. Additionally, the method used for NP estimation is prone to operator's subjective observations, because the NP is evaluated by a visual estimation of sample effervescence after adding HCl, which provokes misleading results. For instance, dolomite ($CaMg(CO_3)_2$) and calcite ($CaCO_3$) have similar neutralizing potential, however, the result from the "fizz test" is quite different because when in contact with HCl, dolomite effervescence is weak or entirely absent. Thus, the NP result for a sample bearing dolomite or calcite as the main neutralizing minerals would be different (Bouzahzah et al., 2015). Additionally, this approach assumes that pyrite is the single sulfur bearing mineral in the sample bringing an overestimated acidity potential in case sulfate and/or non-acid forming sulfides are present in appreciable amount (Bouzahzah et al., 2015). Furthermore, the ABA test is performed on 2 g of pulverized samples and does not consider the initial texture of the mineral material (Elghali et al., 2018).

To overcome these problems, the standard Sobek method has been modified over the years and protocols that take into account mineralogical features have been developed (Bouzahzah et al., 2014, 2015; Lawrence and Wang, 1997; Kwong and Ferguson, 1997; Meek, 1981; Skousen et al., 1997; Jambor et al., 2003; Weber et al., 2004). However, the majority of these improvements have targeted the NP protocol explicitly, leaving the AP methodology lacking in sufficient precision. The only improvement on the AP definition relies on considering the sulfides present instead of the total sulfur. For the NP, on the other hand, the works proposed by Kwong (1993), Lawrence and Scheske (1997) and Paktunc (1999) considered the proportion and the relative reactivity of each neutralizing mineral available in the sample when calculating the NP value. Moreover, the Paktunc (1999) protocol considered the presence of oxidizable cations (Fe, Al and Mn) able to release H^+ during weathering and as a consequence decrease the effective NP. Furthermore, Bouzahzah et al. (2015) suggested a protocol aiming to eliminate the subjectivity of the "fizz test" and define the "fizz rating" in a quantitative manner.

Although these modifications are strengthening the reliability of AMD assessment, they still bear uncertainness because they neither consider the exact mineralogy nor the degree of liberation of acid-generating and acid-neutralizing minerals inside the sample (Elghali et al., 2018). These uncertainties could lead to overestimation of the AP, especially when the presence of non-acid forming sulfides is considerable or when the minerals are locked into inert matrix (Elghali et al., 2019). Finally, the overall AMD behavior of a waste material is a function not only of the balance between acid-generating and acid-neutralizing phases, but is largely influenced by particle size, liberation degree, degree of alteration, morphology and spatial relation between AP and NP phases and between the sulfide minerals themselves (galvanic interaction) (Smith et al., 2000; Parbhakar-Fox et al., 2009; Erguler and Erguler, 2015; Chopard et al., 2017; Elghali et al., 2018). In this context, innovative approaches have been developed based on mineralogical quantification methods bridging mineralogical and textural features of the material to its geochemical behavior. Elghali et al. (2018) suggested to define a diameter of physical locking of sulfides (DPLS) in a way to separate the reactive and non-reactive fraction of a waste rock, whereas Brough et al. (2013) and Parbhakar-Fox and Lottermoser (2015) proposed to characterize the mining waste as "geo-environmental units" or "geo-waste units" based on their geochemical behavior during weathering.

The aim of this study is to improve the understanding of how the geochemical behavior in terms of AMD generation of a sulfide tailings is dictated by mineral reactivity in relation to their liberation degree (e.g., locked, liberated and partially liberated pyrite, explained below in the text). Specific objectives are: (i) to perform flotation of the tailings in a way to pre-concentrate the reactive pyrite as potential contributor to AMD generation, and (ii) to evaluate the efforts to re-classify the tailings from an acid–generating to neutral ones by recalculating their AP based on their intrinsic mineralogical features. An automated mineralogy (AM) analysis has been conducted on two composite samples from DPM-Ch tailings management facility (TMF) and on selected products after pyrite flotation. Additional studies involving static and kinetic tests were prepared to (i) characterize the extent of metals (iron, aluminum) immobilization and release of sulfate ions and their relation to tailings properties, mainly pH and particle size, and (ii) to calculate with more accuracy the quantity of lime (CaO) required to neutralize the acidity produced by pyrite oxidation when environmental desulfurization by flotation is envisaged and the liberation degree of the acid-producing minerals is taken into account.

2. Materials and methods

2.1. Chelopech deposit and mining complex

The Chelopech deposit is located within the northern part of the Panagyurishte metallogenic district, in the central part of the Srednogorie zone - Bulgaria. This mineral province was formed as a result of the calc-alkaline magmatism related to the successive accretion of island arcs during Late-Cretaceous (Stoykov et al., 2002; Georgieva, 2017).

The basement of the Panagyurishte metallogenic district is composed of high-grade metamorphic rocks (two-mica migmatites with thin intercalations of amphibolite), low metamorphic phyllites and granite gneiss. This basement is overlain by the Late Cretaceous volcanic and sedimentary succession. The top of this sequence consists of foreland sediments (Chambefort, 2005; Chambefort and Moritz, 2014). The Chelopech Formation, which hosts the mineralization, is subdivided into lower and upper units. The lower unit shows typical high sulfidation alteration zones and consists of a two-mica volcanoclastic sandstone interfingered with volcanogenic resedimented syn-eruptive breccia (Chambefort, 2005).

The mineralization presents lithological control and can occur disseminated, as veins, stockwork, mineralized breccia and massive sulfide replacements (Chambefort and Moritz, 2014). It is also controlled by the advanced argillic alteration halo, which is characterized by the presence of massive silica, alunite and clay minerals (kaolinite/dickite) (Georgieva et al., 2002). Furthermore, the alteration zones overprinting the country rocks encompass an innermost advanced argillic alteration zone, followed by a sericitic zone and an external propylitic alteration (Georgieva, 2017). These distinct alterations zones corroborated to the interpretation of Chelopech being a high-sulfidation epithermal ore deposit (Chambefort and Moritz, 2014).

Dundee Precious Metals Chelopech (DPM-Ch) mining complex, encompasses an underground mine, a processing plant, a tailings management facility and a paste fill plant. The main target minerals are copper sulfosalts (enargite, luzonite and tennantite) followed by chalcopyrite and minor copper oxides (Rincon et al., 2019); pyrite is recovered due to its association with gold (O'Connor et al., 2018).

The processing flowsheet currently used in DPM-Ch was completed in 2012 and allowed the company to treat around 2 Mt of ore per year. The beneficiation process involves a grinding circuit, bulk sulfide flotation and copper and pyrite flotation circuits. Thus, the two main commodities are a copper and pyrite concentrate. The final tailings are a combination of bulk flotation tailings and pyrite tailings. After

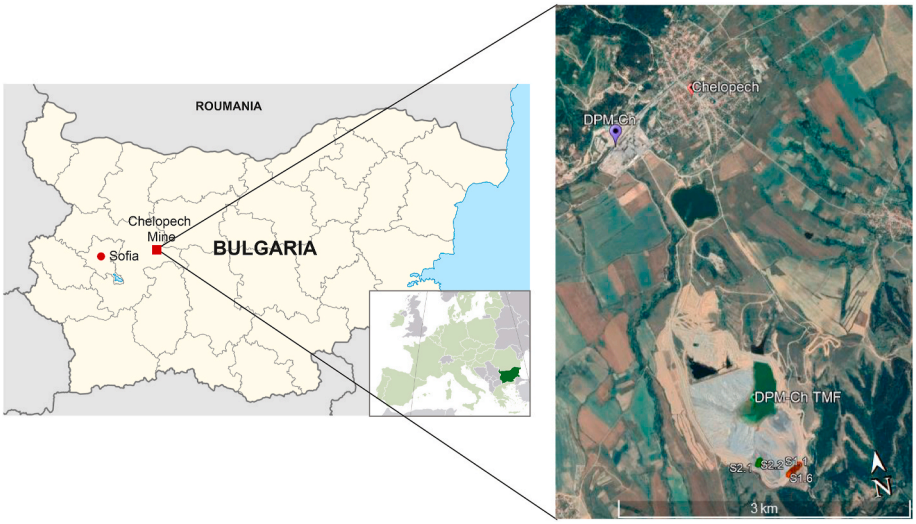

Fig. 1. Sampling location into the Dundee Precious Metals Chelopech tailings management facility.

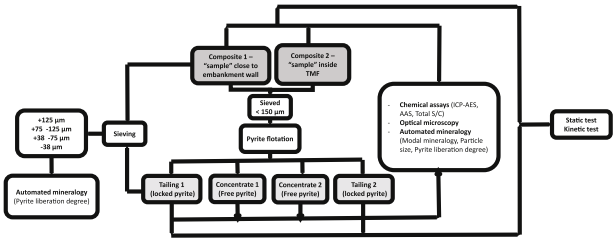

Fig. 2. Experimental and characterization flow to follow the effect of pyrite liberation degree on AMD generation potential.

Table 1
Process parameters used for batch pyrite flotation.

Flotation test ID	Composite sample	pH	PAX (g/ton)	Frother (drops)	Flotation time (min)	Sodium silicate (g/ton)
ULg 1	1	3.1	90	–	11	–
	2	5.7	90	6	11	–
DPM-Ch	1	3.3	50	–	9	–
	2	6	50	6	10	–
ULg 2	1	3	40	–	10	120
	2	5.5	40	–	9	150

thickening, these tailings are diverted either towards the paste fill plant or towards the TMF (O'Connor et al., 2018). Currently, the capacity of the paste plant dictates that about 40% of the overall tailings volume is used as backfill material while 60% is discharged at the TMF (Todorova et al., 2017).

2.2. Sampling and preparation procedure

Two composite samples collected at the TMF belonging to Dundee Precious Metals Chelopech (DPM-Ch) mine were used. The TMF occupies a surface area of about 110 ha and receives annually about 1.2 Mt of tailings material. Composite sample 1 was collected close to the main embankment wall, whereas composite sample 2 was taken from the tailings pond in proximity to a point of discharge (Fig. 1). Fig. 2 depicts the characterization steps and the processing follow-up undertaken for the two samples.

To avoid further oxidation after sampling, the material was immediately dried at 60 °C for 24 h and kept in a refrigerated room. Then, both samples were homogenized and divided into 2 sub-samples. To ensure homogeneity and representativeness of the sub-samples, riffle splitter and/or quartering were used depending on the mass of needed material. The first sub-sample was sent to Liege University (ULg) for mineral characterization and AMD assessment while the second was used for flotation and chemical assays at the DPM-Ch R&D lab. Subsequently, the products from flotation were mineralogically characterized and examined for AMD generation at ULg.

2.3. Chemical assays

Bulk chemical composition of the samples was analyzed at the SGS laboratory located at the mine site. Iron (Fe) was assayed by inductively coupled plasma optical emission spectroscopy (ICP-OES) after aqua regia digestion, analyses for As and Cu were made using an Atomic Absorption Spectroscopy (AAS), whereas total carbon and sulfur content was determined by induction furnace (Leco).

The leachates recovered from the kinetic tests were filtered using a 0.45 µm nylon filter. The filtered leachates were acidified with concentrated HNO3 for sample preservation and analyzed for sulfate ions via ion chromatography (kinetic test explained in section 2.5).

2.4. Pyrite flotation

In order to assess the influence of pyrite liberation degree on AMD generation, three flotation tests were performed at slightly variable flotation regimes with a common aim to find out the conditions leading to an optimum flotation yield of the reactive pyrite while keeping the locked one in the tailings. Two flotation tests were accordingly performed in ULg and one at the DPM-Ch facility. Before flotation, composite samples 1 and 2 were dry sieved using a Ro-Tap sieve shaker to eliminate the 150 µm oversize fraction. No attempt was made to refresh particle surfaces therefore samples were not reground. The flotation was performed in a 2-L Denver laboratory machine using each time 500 g as feed. The collector was PAX (potassium amyl xanthate) supplied at different dosages, while MIBC (methyl isobutyl carbinol) was used as frother. No reagent was added to control pH. Table 1 summarizes the process parameters used during the batch flotation tests performed at both labs.

To mimic industrial conditions, the batch flotation performed at DPM-Ch lab was undertaken using process water from the plant, whereas the tests at ULg lab were performed with tap water. The first orientation trials (referred as ULg 1) were done under addition of collector in amount higher than usual (90 g/T) and flotation was run until froth loading was clear. The reason was to guarantee elimination of the

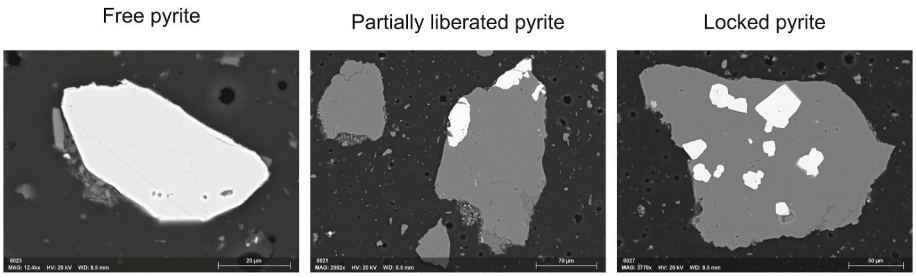

Fig. 3. Backscattered images showing the three different grades of pyrite liberation.

entire amount of free pyrite. The optical microscope inspection of the concentrate revealed however that both locked and liberated pyrite floated. Therefore, collector dosage and flotation time were reduced. These steps led to better flotation recovery of free from locked pyrite. The trend was particularly pronounced for composite 1 sample. Moreover, dispersant was introduced at the ULg 2 test to decrease the amount of agglomerate observed. However, this measure did not improve the efficiency.

2.5. Mineralogical characterization

After each flotation test, the recovered products were dried and a representative sample mounted in an epoxy polished block for observation under a reflected light microscope (ZEISS AxioImager M2m). The optical inspection enabled visualization of the extent to which liberated pyrite was recovered in the concentrate and if locked pyrite remained in the tailings. Detailed mineralogical investigation was addressed using a ZEISS Automated Mineralogy "Mineralogic" system yielding modal mineralogy, particle size distribution and pyrite liberation degree. The Mineralogic system is equipped with two Bruker xFlash 6|30 x-ray energy dispersion spectrometers (Silicon drift detector). The SEM-EDS analyses were carried out using a probe current of 2.3 nA with an accelerating voltage of 20 kV at a working distance of 8.5 mm. A mapping mode was performed using a 3–5 μm step size and a dwell time of 55 ms. Magnification was set to 1300 and a total of 5000 particles were analyzed on each sample. The "Mineralogic" system gave as output BSE (backscattered secondary electrons) images and a fully quantitative EDS analysis. For data processing, a minimum and maximum ranges for elements occurring in the mineral formula were defined and a specific gravity for each mineral was selected. Following data processing, the elemental ranges found in the minerals were further refined for optimal mineral distinguishing and classification. Automated mineralogy (AM) was also performed on sieved fractions from composite 1 and tailings 1 of DPM-Ch test. The reason for focusing on composite sample 1 only was its better behavior in terms of free pyrite concentration by flotation.

2.6. Acid mine drainage assessment

2.6.1. Static test

The NP of the studied samples was determined using the sequential HCl addition protocol as proposed by Bouzahzah et al. (2015). The method consists in placing 1 g of sample into a 250 mL flask with 50 mL of deionized water at room temperature. The flask is then introduced onto a rotary shaker run at 220 rpm and the initial pH (t = 0 h) is registered. The pH is measured after 2 h and adjusted to 1.8 ± 0.02 (initial pH). The pH is further documented after 24 h and maintained (by HCl addition) around the initial value (pH = 1.8 ± 0.02). These steps are repeated until reaching steady-state conditions for 24 h (meaning complete digestion of the neutralizing minerals). The solutions are then filtered using a 0.45 μm nylon filter and titrated under constant stirring to pH 5. Thereafter, 5 mL of 30% H_2O_2 is added to the solution to oxidize all available oxidizable cations (Fe, Mn, Al). After 1 h, the solution is back titrated with 0.1 N NaOH to pH endpoint of 7, then portion of 50 μL of H_2O_2 is added to each solution and the pH measured again. This procedure is repeated until no change in pH observed for 10 min. The samples are kept overnight and pH recorded in the following morning. The process of titration until pH 7, H_2O_2 addition and letting the sample react overnight is repeated until reaching stable pH of 7 for more than 24 h. The NP is calculated by equation (1).

$$NP = \frac{50a\left[x - y\left(\frac{b}{a}\right)\right]}{m} \quad (1)$$

Where:

a, b: normality of HCl and NaOH respectively (N)
x, y: volumes of added HCl and NaOH respectively (mL)
m: sample weight (g)

The acid-generating potential (AP) is calculated based on the total sulfur content, ($AP = 31.25^{*}$ % $S_{\text{total sulfur}}$) and thereafter the information acquired by the automated mineralogy is used to calculate the effective AP of the samples. In such a way only the amount of accessible sulfur (liberated pyrite) is effectively considered. In practice, the pyrite content is transformed into sulfur grade and multiplied by pyrite liberation degree, as illustrated by equation (2):

$$\text{Effective AP} = X_i \times L_p \times 0.5345 \quad (2)$$

Where:

Xi : Pyrite content in the sample (Wt.%)
Lp: percentage of reactive pyrite in the sample (100 - locked pyrite) (%)
0.5345 : pyrite to sulfur conversion factor

The AP and NP are expressed in kilograms of $CaCO_3$ equivalent per ton of sample (kg $CaCO_3$/t). There are two standard methods used to classify the waste material regarding its acid generating potential: the neutralization potential ratio (NPR = NP/AP) and the net neutralization potential (NNP=NP-AP). In this work, we will use only NPR as classification criterion. Thus, when the NPR is greater than 2, the sample is considered as non-acid generating; when the NPR is lower than 1, the sample is considered as acid-generating; and when the NPR is between 1 and 2, the sample is considered as uncertain.

2.6.2. Liberation degree of pyrite

The liberation degree of minerals is commonly used in the field of mineral processing. It is generally agreed that a liberated particle is one that contains only one mineral. By extension, particles which contain two or more minerals are described as partially liberated, locked or composites particles. In this study, "liberated" minerals (or grains) are typically those with the 80–100% liberation degree in the containing particles, "locked" minerals are those with liberation degree lesser than 20%, and in between, are "partially liberated" particles. In this paper, we consider that the pyrite with liberation degree greater than 20%

Table 2
Composition, granulometry and mineralogy of head composite samples and flotation products.

Head samples					DPM-Ch flotation products			
Characterisation	Parameters	Units	Composite 1	Composite 2	Composite 1		Composite 2	
					Concentrate 1	Tailing 1	Concentrate 2	Tailing 2
Chemical assay	S	(wt. %)	8.41	5.67	38.3	3.34	10.8	5.1
	C		0.004	0.046	–	0.011	–	0.032
	Fe		7.85	5.38	32.8	2.58	9.44	5.11
	Cu		0.13	0.12	0.5	0.05	0.38	0.11
	As	(ppm)	243	231	751	140	969	185
Bulk mineralogy by AM	Quartz	wt. %	49.7	56.0	13.7	63.1	26.3	61.3
	Kaolinite		26.2	24.5	6.8	24.4	32.1	17.3
	Muscovite		3.8	3.9	0.7	3.7	3.1	7.5
	Other silicates		3.4	3.6	0.9	1.4	5.8	3.08
	Carbonates		0.002	0.05	0.00	0.01	0.02	0.09
	Pyrite		16.1	11.1	77.4	6.3	30.0	9.1
	Other sulfides		0.08	0.17	0.21	0.02	1.39	0.06
	Rutile		0.19	0.23	0.08	0.16	0.12	0.15
	Barite		0.45	0.26	0.15	0.75	0.84	0.74
	Traces		0.10	0.18	0.01	0.22	0.49	0.64
Granulometry	d_{20}	µm	14	9		7		10
	d_{50}		38	28		13		25
	d_{80}		99	68		46		58
	d_{95}		191	95		67		96
Pyrite liberation degree	Liberated	%	27.4	45.3	76.1	35.3	40.8	61.7
	Partially liberated		52.1	31.1	21.8	33.5	46.8	26.1
	Locked		20.6	23.6	2.0	31.2	12.4	12.2
	Reactive pyrite		79.5	76.4	97.9	68.8	87.6	87.8
Static test results	Volume HCl	mL	1.5	1.3		1.1		1.3
	NP	kg $CaCO_3$/t	7.5	3		0.1		1.5
	AP		263	177		104		159
	NPR (=NP/AP)		0.03	0.02		0.0001		0.009
Static test correction	Effective AP		208	135		44		134
	AP-effective AP		55	43		60		50

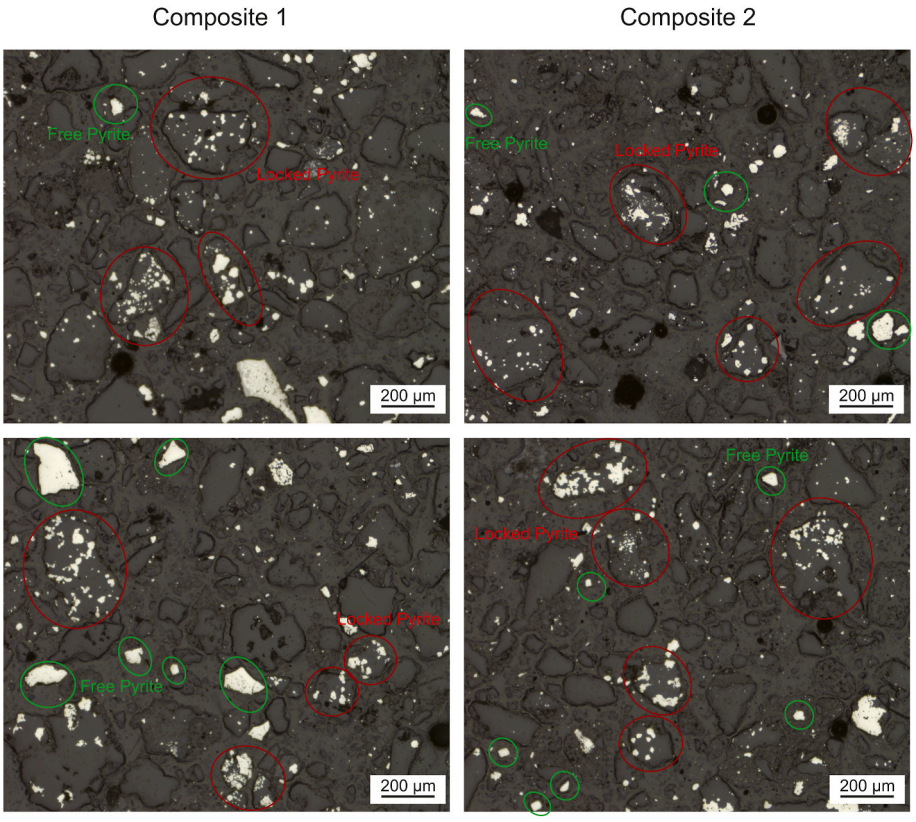

Fig. 4. Optical microscopy (reflected light) view of the studied composite samples highlighting the presence of free and locked pyrite (dark phases are gangue minerals and bright phases represent sulfide minerals).

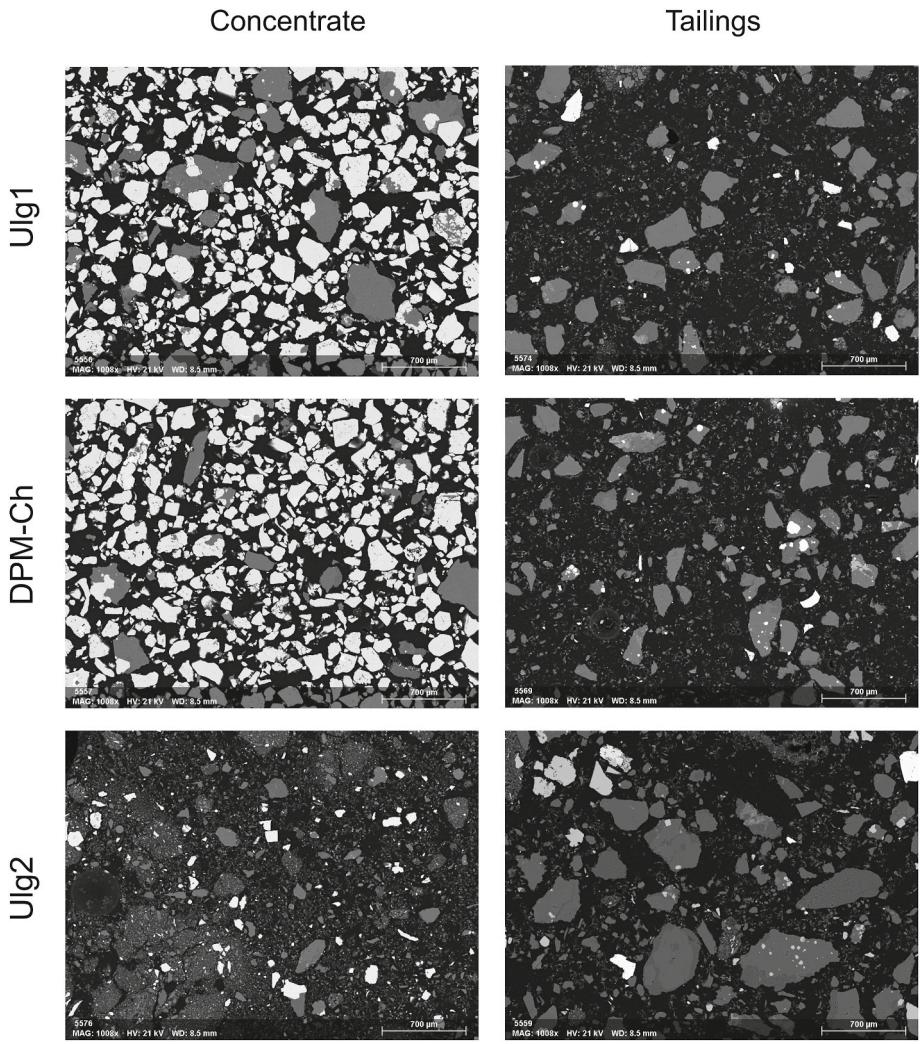

Fig. 5. Backscattered images of concentrates and tailings after pyrite flotation (Gangue minerals are dark gray phases and sulfide are bright phases).

Table 3
Pyrite liberation degree after sizing - pyrite is considered as liberated when more than 80% of its surface area is exposed; partially liberated when pyrite have between 20% and 80% of its surface area exposed; and locked when less than 20% of its surface area exposed; the partially liberated and liberated fractions were considered as reactive pyrite.

	After sieving and with AP correction based on liberation degree									
	Composite 1					Tailing 1				
	+125	+75	+38	−38	Reconstructed	+125	+75	+38	−38	Reconstructed
Liberated	29.6	63.2	82.9	92.9	58.0	6.3	19.5	65.3	86.5	23.0
Partially liberated	27.4	23.5	12.6	5.9	21.0	21.8	23.0	10.3	8.5	19.0
Locked	43.0	13.3	4.5	1.1	21.0	72.0	57.5	24.4	5.0	58.0
Reactive pyrite	57.0	86.7	95.5	98.8	**79.0**	28.1	42.5	75.6	95.0	**42.0**

(liberated and partially liberated) will be fully reactive. However, the pyrite grains with liberation degree lesser than 20% are considered locked and are not reactive. As displayed in Fig. 3, within the "locked" pyrite liberation grade, only a very limited part of the entire pyrite surfaces is exposed to oxidation and acidity generation.

2.6.3. Kinetic test

In order to validate the results obtained by the ABA static test while taking into account pyrite liberation degree, kinetic tests were performed on both flotation feeds (composite 1 and 2) and the resulting tailings from "DPM-Ch flotation" test (tailings 1 and 2, Table 1) using a small-scale humidity cell tests (Cruz et al., 2001) modified by Bouzahzah et al. (2014). For the original small-scale humidity cell, 67 g of dry sample is placed on a fiber filter fixed on a 10 cm Buchner filter funnel and a 7-day leaching cycle was performed. The 7-day leaching cycle consists of flushing the samples with 50 mL deionized water on the first day, followed by 2 days of exposure to ambient air. On the fourth day, the samples are leached again followed by 3 days of air exposure. During each flush, the deionized water is left in contact with the samples for 3 h and then recovered by suction using a filtering flask. In our study, the leached solutions are weighed and 20–30 mL of the leachate filtered using a 0.45 µm nylon filter. The filtered leachates are acidified with concentrated HNO_3 for sample preservation and analyzed for sulfate (SO_4), Fe, Cu, As and Al. The pH and Eh of the leachate are immediately

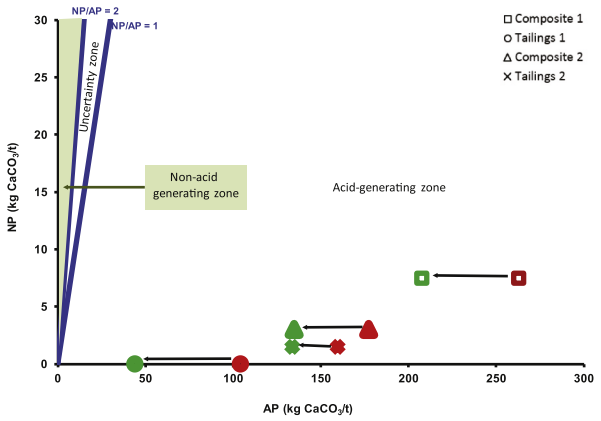

Fig. 6. Samples classification in terms of AP and NP when using a static test (red mark) and an effective AP after correction accounting the pyrite liberation degree (green mark). (For interpretation of the references to colour in this figure legend, the reader is referred to the Web version of this article.)

measured and acidity and alkalinity determined using standard titration (NaOH 0.1 N for acidity determination and H_2SO_4 0.01 N for alkalinity determination). The modification suggested by Bouzahzah et al. (2014) consists of maintaining the optimal conditions for oxygen diffusion and keeping the samples close to the optimal saturation level for sulfide oxidation (between 40% and 60%) during the entire test. During this work, a total of 11.5 cycles were performed (the test was run for 81 days).

3. Results and discussion

3.1. Composite (feed) samples characteristics

The composite samples collected from the TMF are characterized by high sulfur and very low carbon contents (Table 2). The mineralogical observations using optical microscopy under reflected light mode showed predominance of gangue minerals in both samples (dark gray, Fig. 4). The modal mineralogy shows that the gangue minerals are mainly silicates (quartz and kaolinite with minor muscovite, plagioclase, biotite and garnet). Very low quantities of carbonate minerals (calcite/dolomite) are measured (ca. 0.01 wt %) which corroborate well the low carbon content reported by chemical assay (<0.1 wt %).

Pyrite is the main sulfide mineral (brighter phase, Fig. 4), whereas copper sulfides (chalcopyrite and bornite) and sulfosalts (enargite and tetrahedrite) are present in trace amounts (ca. 0.1 wt %). Both samples contain free and locked pyrite, with the locked one being mainly associated with the silicate minerals, mainly to quartz (Figs. 4 and 7).

The granulometry and the pyrite liberation degree obtained by the AM are likewise summarized in Table 2. The granulometric data suggest that both samples could be classified as fine grained materials (d_{80} < 100 μm). Composite sample 1 presents a coarser and slightly broader particle size distribution with higher amount (79.5%) of reactive pyrite than the one in composite 2 with 76.4% of reactive pyrite. To note that under "reactive", we induce the amount of pyrite as "fully liberated" and the one classified as "partially liberated" (e.g. grains with more than 20% of pyrite exposed area).

3.2. Flotation products characteristics

The high collector concentration and long flotation time used for the first flotation test (ULg 1) resulted in the flotation of both free and locked pyrite whereas a limited amount of very fine grains (mostly free pyrite) remained in the tailings (Fig. 5). In order to prevent the flotation of locked pyrite, the collector dosage and flotation time were lowered for the followings tests.

Although dispersant was introduced in ULg 2 test aiming to decrease the amount of agglomerates observed in the head samples, this test did not achieve the desired selectivity, as the optical inspection of ULg 2 flotation products confirmed that free pyrite reported to the tailings whereas gangue minerals floated (Fig. 5).

The use of process water in the DPM-Ch flotation test immediately reflected in a higher pulp pH. The microscopic observations of the DPM-Ch flotation products reveal that a large part of the locked pyrite remained in the tailings while the liberated one floated (Fig. 5). The free pyrite was not entirely recovered because fine sized grains are still seen lost with the tailings. Based on these findings, the AMD-oriented characterization and geochemical tests were further extended only on the DPM-Ch flotation products.

Table 2 summarizes the chemical and mineralogical characteristics of the DPM-Ch flotation test products. Because the objective was to follow the pyrite behavior, a particular focus is placed on sulfur content and pyrite variation between the composite samples (flotation feed) and the flotation products. When comparing the chemical assays, it is possible to observe that sulfur in tailings 1 (3.3 wt %) is much lower than in composite 1 (8.4 wt %), whereas sulfur content in tailings 2 is similar

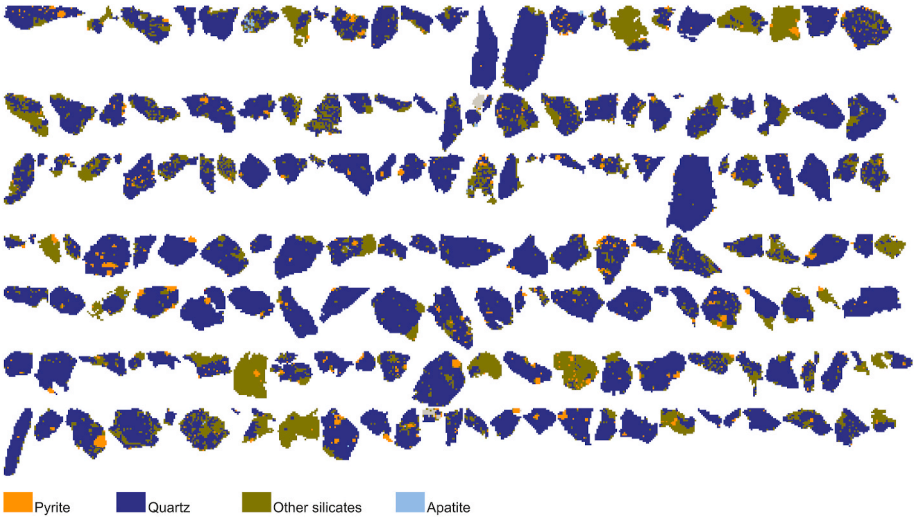

Fig. 7. Automated mineralogy filter displaying the only "locked pyrites" grade showing that the fully locked pyrites are considerably higher in number than the partially locked pyrites.

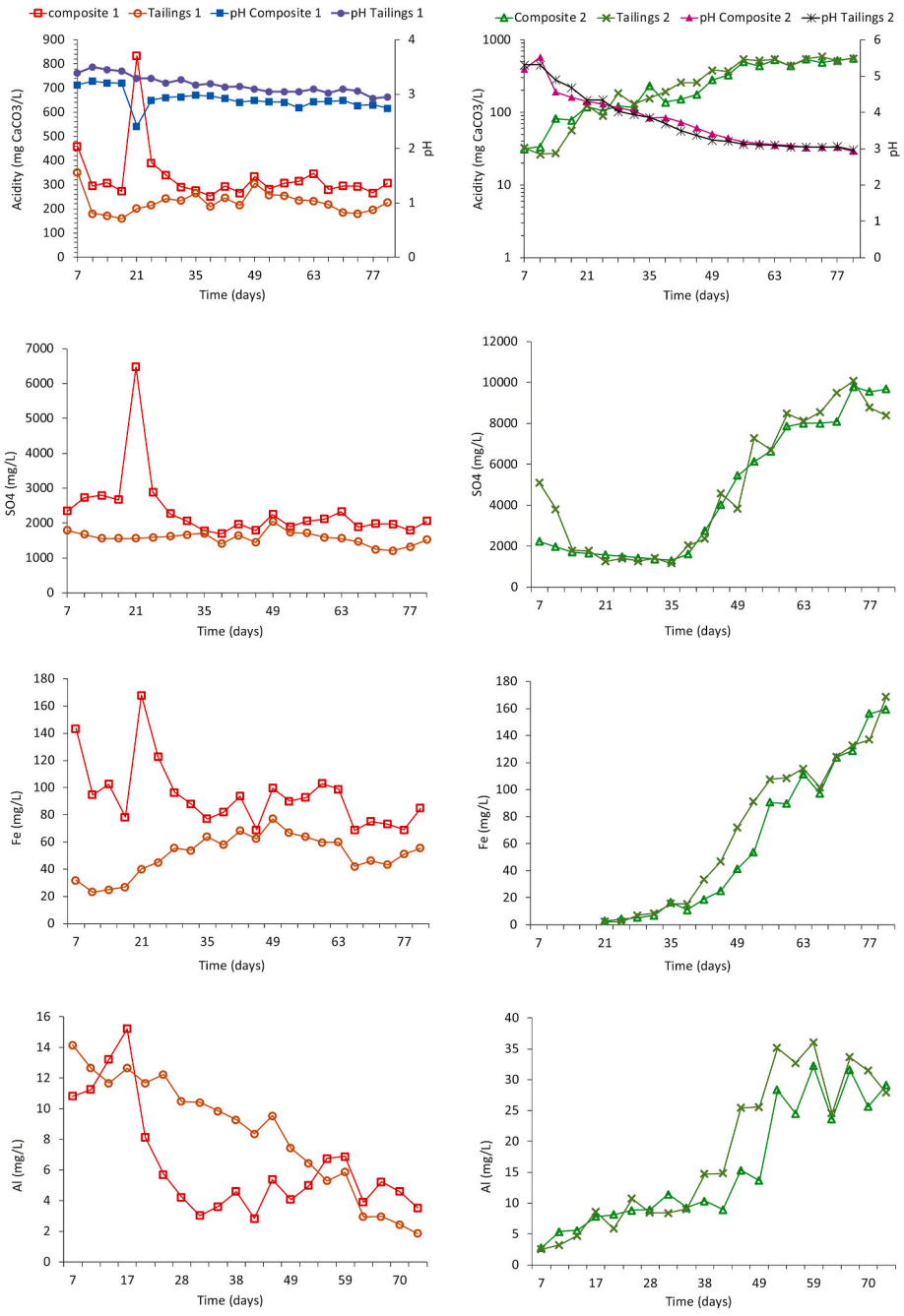

Fig. 8. Evolution of pH, acidity and punctual leaching curves for sulfate, Fe and Al.

(5.1 wt %) to that in composite 2 (5.7 wt %). Thus the chemical composition confirmed the trend delivered quantitatively by the automated mineralogy in the sense that pyrite decreased from 16.1 wt % to 6.3 wt % in composite sample 1 and from 11.1 wt % to 9.1 wt % in composite 2.

The granulometric distribution (d_{20}, d_{50}, d_{80} and d_{95}) and the pyrite liberation degree of the products coming from the DPM-Ch flotation test are also displayed in Table 2. Among the studied samples, tailings 2 appears as the most reactive, with 88 wt % pyrite available for reaction, whereas tailings 1 has the lowest amount of available pyrite (69 wt %). Moreover, tailings 2 is coarser than tailings 1 with d_{50} of 25 μm d_{80} of 58 μm, whereas the d_{50} for tailings 1 is found as 13 μm and d_{80} as 46 μm.

3.3. Flotation performance

As a rule, flotation performance is influenced by variety of factors, such as particle size, degree of mineral oxidation, type and concentration of reagents, water chemistry, pulp physico-chemistry (pH and Eh) (Wills and Finch, 2016). Among these parameters, the composition of the process water and presence of ions, which can activate or depress a mineral, plays a significant role.

The results from the chemical assay and the automated mineralogy, depicted in Table 2, are evidencing the differences in pyrite flotation between composite 1 and composite 2. While flotation was capable to effectively decrease the sulfur content in tailings 1, for composite 2 flotation seems to be less selective. The observed difference in flotation behavior could be attributed to the different pH under which flotation was performed (Table 1). Pyrite flotation using relatively low dosage of

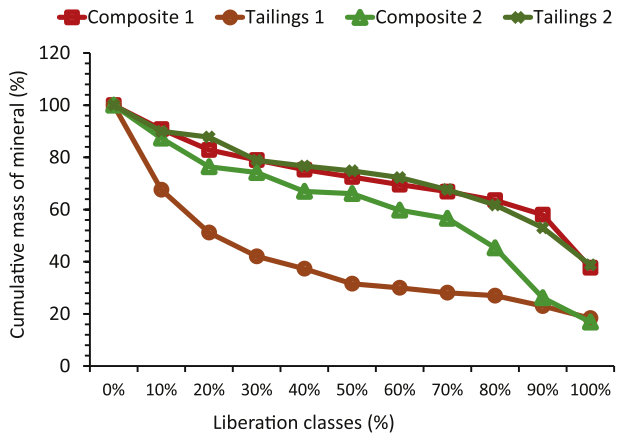

Fig. 9. Liberation degree of pyrite in the four samples submitted to kinetic test.

collector (e.g., xanthate) could be practiced at two distinct pH regions: either around pH 4 or 9, whereas at pH below 2, higher than 11 and between 5 and 7 pyrite tends to be depressed (Fuerstenau et al., 2007). These findings corroborate with the efficient pyrite flotation observed around pH 3.3 and with the lower efficiency when pH is close to 6.

Another factor that might have contributed to the observed flotation differences is the possible activation of pyrite by copper ions at low pH (Zhang et al., 1997). Both composite samples have Cu-bearing minerals, even in low quantity. These minerals are prone to oxidation at low pH and the Cu (II) leached from the mineral lattice could be responsible for activating pyrite. Additionally, the available iron (III) could act as an oxidizing agent for copper, bringing it in solution and likewise enhancing pyrite activation. Hence, it could be assumed that pyrite flotation from composite sample 1 is strongly influenced by combination of these factors.

3.4. Pyrite liberation degree derived from automated mineralogy

In order to follow closely the liberation degree of pyrite in terms of granulometric repartitioning, composite 1 and tailings 1 from the DPM-Ch flotation test were sieved at 38 μm, 75 μm and 125 μm classes and polished blocks were prepared for each fraction (<38 μm, +38/-75 μm, +75/-125 μm and >125 μm). A mapping mode analysis was done at 3–5 μm step size depending on sample's granulometric tranche with an acquisition time (dwell time) of 55 ms per step. The pyrite liberation degree obtained for each size fraction and the frequency of the size class were used to recalculate the degree of pyrite liberation for the entire composite sample using equation (3) (Elghali et al., 2018):

$$\%L = \sum c_i \times \frac{A_i}{100} \tag{3}$$

where:

Ci: average liberation class
Ai: frequency of class Ci

The pyrite liberation degree in each granulometric fraction is displayed in Table 3. As grain size increases, the liberation degree decreases. As a consequence, for both composite 1 and tailings 1, pyrite could be mostly found as liberated in the "finer" classes: 38 μm and +38 μm/-75 μm. This result could be related to the well-known difficulties in floating particles within this fine size range. The assumption could be further supported by the fact that for the "coarser" size classes (e.g., +75 μm), most of the free pyrite floated. Furthermore, the amount of reactive pyrite calculated for each sample after sieving shows that the degree of liberation for composite 1 is not affected by sieving, whereas for tailings 1 the amount of reactive pyrite dropped from 69% to 42%.

3.5. AP and NP coming from static tests

Composite 1 and 2 and tailings 1 and 2 were subjected to static test investigation. The NP was determined through a sequential HCl addition. On the other hand, the AP, was calculated based on the total sulfur content given by the chemical assay. The results from the static test are depicted likewise in Table 2 which provides a comparative overview of the results from all tests. The data provision therefore encompasses: volume of HCl required to digest the samples; NP value calculated by back-titration; AP calculated based on sulfur grade; and NPR ratio. The lack of neutralizing minerals (carbonates only about 0.01 wt %) confirmed by the very low carbon content in all the samples, reflects a very low NP value (<8 kg $CaCO_3$/t). As a consequence, the NPR of all the samples is ranging between 0.0001 and 0.003 rendering all of them as acid-producing.

3.6. Static test results corrected with pyrite liberation data

The traditional Sobek test (Sobek et al., 1978) assumes that the entire amount of sulfur in the sample is available for oxidation. Indeed, the sulfur in the studied samples should come only from pyrite and it should be deriving from the reactive fraction. The AM results confirmed the first hypothesis but it has shown that part of the pyrite is locked, thus the Sobek test would tend to overestimate the acid generating potential of the samples. In order to overcome this issue, the AM output was used to calculate the "effective AP" of the samples and the corresponding readjusted data is presented in Table 2. The NP is considered as the same as the one defined by the Sobek test modified by Bouzahzah et al. (2015).

Fig. 6 shows the graphical comparison between the result from the Sobek-based static test and the results corrected by automated mineralogy (effective AP). The graph illustrates the tendency of the traditional static test to overestimate the AP when part of the pyrite is locked inside gangue grains and as therefore not accessible to oxidation. In such a way, the calculated difference between the AP (defined by the Sobek test) and the effective AP (corrected with AM findings) for composite 1 and tailings 1 respectively is 55 and 60 kg $CaCO_3$/t. Similarly, the same balance for composite 2 and tailings 2 arrives as 43 and 50 kg $CaCO_3$/t respectively. Therefore, if one takes into account the liberated pyrite only, it becomes possible to shift all the samples from the acid generating zone towards neutral one. In our samples, as they have no neutralizing potential, the samples remained acidic but should generate less acidity as part of the pyrite is unavailable for oxidation. Fig. 7 shows all the pyrite particles classified as locked by the AM. It can be seen that most pyrite grains are fully locked within quartz, which is an inert mineral.

To verify if the weathering response of the samples likewise depends on pyrite liberation degree, kinetic tests were performed as next step.

3.7. Kinetic test results

The kinetic test conducted in weathering cells has served to confirm the ABA forecast obtained by the static test using the AM results. The acidity evolution of the leachates recovered from the weathering cells is shown in Fig. 8. The acidity and the dissolved elements released by all the samples during the first two flush cycles are relatively high mainly due to phenomena provoking the leaching of weakly-bond soluble elements initially present in the samples and could be related back to in-situ oxidation in the pond (therefore they are not displayed in Fig. 8). After the first two flushes, the recorded acidity and the dissolved elements are documenting an instant reactivity of the samples when submitted to the kinetic test.

The initial acidity released by composite 1 and tailings 1 is two orders of magnitude higher than that of composite 2 and tailings 2. The acidity curves for composite 2 and tailings 2 show a continuous increase in acidity and after 45 days, tailing 2 turns the sample releasing the highest acidity. When compared to composite 2, the elevated acidity

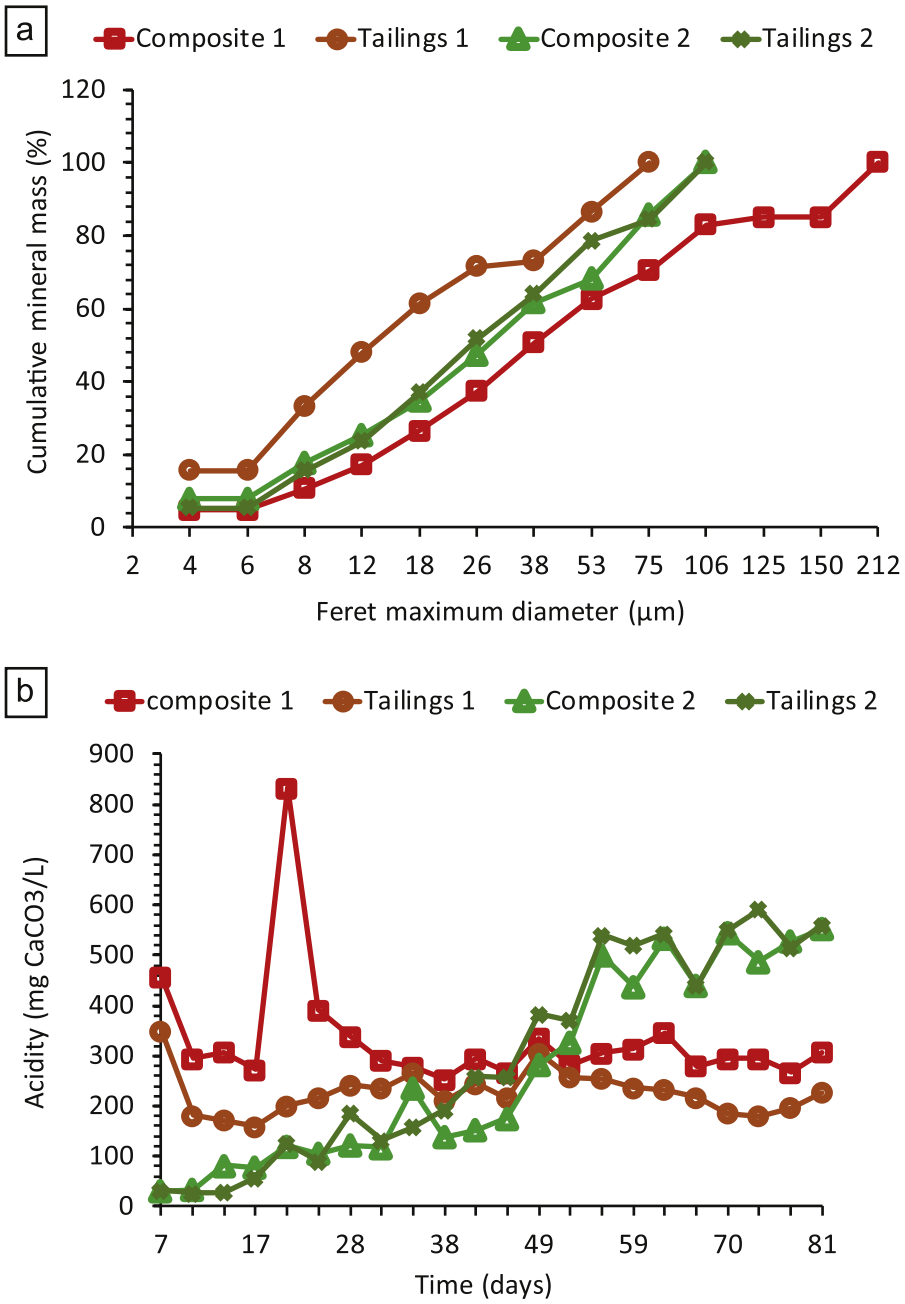

Fig. 10. (a) Particle size distribution of pyrite as given by the automated mineralogy and (b) acidity release with time, for the four samples submitted to kinetic tests.

generated by tailings 2 is most likely due to the largest amount of reactive pyrite (Table 2), thus confirming that mine tailings reactivity and their acidity generation capacity are ultimately influenced by the pyrite liberation degree. Moreover, as seen in Fig. 8, the level of acidity release by the leachates correlated well with pH. Indeed, for composite 1 the decrease in pH at day 21 is due to the higher rate of pyrite oxidation (e.g., sulfate release) and the continuous production of sulfates by composite 2 and tailings 2 is logically followed by continuous drop in pH for these samples.

Fig. 8 also shows the evolution over time in the concentrations of sulfate, iron and aluminium in composite samples 1 and 2 and their respective tailings. The recorded levels of released sulfate in the leachates correlates well with pH and acidity curves. Composite 2 and tailings 2 had a continuous increase in sulfate loads reaching 10,000 mg/L, whereas composite 1 and tailings 1 displayed constant sulfate production up to around 2000 mg/L. The iron and sulfate ions in the leachates are coming from pyrite oxidation with a respective trend confirming the distinct behavior for composite 1 and 2 and tailings 1 and 2. Iron is leached continuously from composite 1 and tailings 1, whereas iron was absent in the first leaching cycles of composite 2 and tailings 2 and starts to be mobilized only after 20 days when pH reached values below 4. Aluminium follows virtually the same behavior as iron, with the exception of emerging in the leachates after the first two cycles. The total absence of iron and aluminum in the first flushes of composite 2 and tailings 2 could be explained by the solubility curve of these elements. They are known to stay immobilized at pH close to neutral (pH 6). Hence, despite being dissolved, these two elements precipitate as oxi-hydroxides and are not present in the leachate. However, when the leachates reach pH below 4, Al and Fe started to appear.

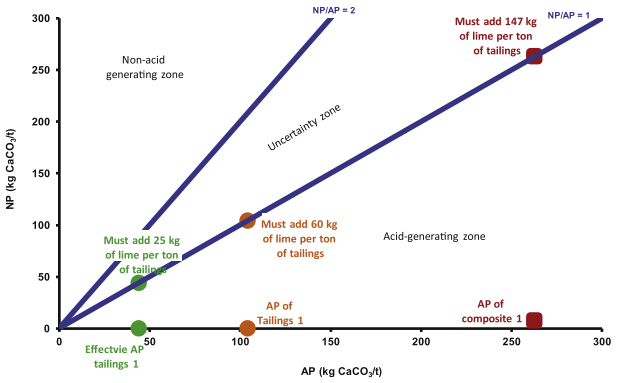

Fig. 11. Transitional path targeting the neutralization of current acid generating tailings.

3.8. Comparative acid generation potential of the tailings

There is a clear indication that the geochemical behavior of the samples during weathering is highly dependent on their textural parameters. The degree of liberation of a given mineral could be translated as expression of its exposure level. Liberated particles are more reactive than the partially liberated ones, whereas fully locked particles are not available for reaction (Elghali et al., 2018). Fig. 9 depicts the pyrite liberation scheme for the four samples submitted to kinetic tests. In fact, the pyrite liberation curve in tailings 2 shows that pyrite is more liberated than in composite 2, which explains its greater reactivity, as confirmed by the results of the acidity produced by this sample. Similarly, the pyrite liberation curve in tailings 1, shows that pyrite is less liberated than in composite 1, resulting in a lower acidity and dissolved elements generation than in composite 1.

Fig. 10a is displaying the reconstructed particle size distribution (PSD) curves for the pyrite (from the automated mineralogy study) in the four samples submitted to the kinetic tests. It should be noted that composite 2 and tailings 2 are characterized by similar particle size distributions and despite that, composite sample 2 shows slightly higher pyrite content (11 wt % against 9 wt % for tailings 2), at the end of the test, tailings 2 released more acidity and generated higher sulfate, iron and aluminium loads (Fig. 8) due to the greater proportion of reactive pyrite (88% in tailings 2 and 76.4% in composite 2). Therefore, pyrite liberation degree seems to be an important parameter impacting the geochemical behavior of composite sample 2 and tailings 2. On the other hand, composite 1 is richer in pyrite (16 wt %) than tailings 1 (6.3 wt %) and because its reactive pyrite content (79%) was higher than that in tailings 1 (42%), it logically produced more acidity and dissolved ions than tailings 1 (Fig. 8). These results illustrate in a very convincing way how pyrite oxidation level is linked to its liberation degree and as a consequence to the overall acidity generation.

Because the surface area available for reaction depends on particle size it is imperative to consider the particle size distribution as a key factor in assessing AMD risks of mine tailings. Finer fractions are as a rule more reactive than coarser ones and therefore they tend to oxidize faster. Looking at Fig. 10a, it could be appreciated that the pyrite in composite 1 is coarser than that in tailings 1, whereas composite 2 and tailings 2 curves are overlapping in almost the entire granulometric range. The acidity evolution with time displayed in Fig. 10b is showing, that at the end of the test composite 2 and tailings 2 are producing higher amount of acidity than tailings 1, even though the pyrite in the latter appears as the finest grained one. This highlights again the strong link between pyrite liberation degree and sample reactivity. Indeed, whereas the pyrite belonging to tailings 1 is characterized by the finest PSD and hence more prone to oxidation, the sample bears the lowest amount of reactive pyrite with only 42% available to oxidation compared to the rest samples where reactive pyrite is between 76% and 88%.

The almost nonexistent intrinsic neutralization potential (NP) of the samples dictated by their mineralogy imposes an adequate AMD management strategy to be practiced at the DPM-Ch mine site. The AMD prevention and control are therefore realized by lime (CaO) addition to maintain pH around 8 in the TMF. The known principle behind this approach is neutralizing the acidity produced by pyrite oxidation and immobilizing the metals under alkaline conditions. Fig. 11 is illustrating the effort needed, in terms of lime addition, to shift the process tailings from the acid generation zone towards neutral tailings. It could be estimated that, based on the 1736 kg $CaCO_3$/t calculated NP of the lime (determined by Sobek test), one has to add 147 kg of lime to neutralize one ton of composite 1 material (having AP = 263 kg $CaCO_3$/t). Whereas to neutralize 1 ton of tailings 1 (the desulfurized part of composite 1) which has an AP of 104 kg $CaCO_3$/t, one needs to use 60 kg of lime only. Furthermore, if the degree of pyrite liberation is taken into account, only 25 kg of lime will be needed to neutralize the acidity from one ton of tailings (effective AP of 44 kg $CaCO_3$/t). This example further confirms the economic importance to consider pyrite liberation degree when quantifying the alkaline agents to deploy during AMD mitigation measures.

4. Conclusions

The presented results reaffirm the importance to consider mineralogical, textural and physical properties of the acid generating minerals when evaluating the geochemical phenomena in management sulfide mine tailings and when choosing the control strategy to mitigate associated environmental impacts. Using mineralogy-based correction the projected amount of alkaline agents for AMD neutralization could be accurately forecasted, which has a direct impact on mine economics.

Although preliminary, the following conclusions can be drawn, which could be likewise used as guidelines in handling AMD related issues linked to handing sulfidic mine tailings:

- An integrated approach that combines mineralogical and geochemical tests should be used to better predict the AMD potential of sulfide mine tailings.
- The AMD potential of the tested process tailings depends strongly on its mineralogical and textural characteristics.
- The absolute AP defined by the traditional Sobek method overestimates the effective AP when pyrite is partially locked (tailings 1).
- The response to weathering of the tailings depends on sulfides liberation and their particle size.
- The geochemical behavior of a bulk sample is dictated by the most reactive fraction of sulfide minerals.
- The amount of lime required to neutralize the acidity produced by pyrite oxidation could be considerably reduced (in our case nearly 4 times) if an environmental desulfurization is envisaged and the liberation degree of the acid-producing minerals considered.

The above findings could be very relevant to upscaling remediation projects in general mine waste management.

Declaration of competing interest

The authors declare that they have no known competing financial interests or personal relationships that could have appeared to influence the work reported in this paper.

Acknowledgments

CM wishes to acknowledge the study fellowship under the ERASMUS-MUNDUS International Master Program on Resources Engineering – EMERALD. The authors would like to thank to DPM-Chelopech mine for their support and the permission to present the results.

References

Blowes, D., Ptacek, C., Jambor, J., Weisener, C., 2003. The geochemistry of acid mine drainage. Treatise Geochem. 9, 612.

Blowes, D.W., Jambor, J.L., Alpers, C.N., 1994. The Environmental Geochemistry of Sulfide Mine-Wastes, vol. 22. Mineralogical Association of Canada.

Bouzahzah, H., Benzaazoua, M., Bussière, B., Plante, B., 2013. Acid-generating potential calculation using mineralogical static test: modification of Paktunc equation. Mise en garde 65.

Bouzahzah, H., Benzaazoua, M., Bussiere, B., Plante, B., 2014. Prediction of acid mine drainage: importance of mineralogy and the test protocols for static and kinetic tests. J. Miner. Water Environ. 33, 54–65.

Bouzahzah, H., Benzaazoua, M., Bussiere, B., Plante, B., 2015. A quantitative approach for the estimation of the "fizz rating" parameter in the acid-base accounting tests: a new adaptations of the Sobek test. J. Geochem. Explor. 153, 53–65.

Broadhurst, J.L., Harrison, S.T.L., 2015. A desulfurization flotation approach for the integrated management of sulfide wastes and acid rock drainage risks. In: Paper Presented at the 10th International Conference on Acid Rock Drainage & IMVA Annual Conference, Santiago, Chile.

Brough, C.P., Warrender, R., Bowell, R.J., Barnes, A., Parbhakar-Fox, A., 2013. The process mineralogy of mine waste. Miner. Eng. 52, 125–135.

Chambefort, I., 2005. The Cu–Au Chelopech Deposit Panagyurishte District, Bulgaria: Volcanic Setting, Hydrothermal Evolution and Tectonic Overprint of a Late Cretaceous High-Sulfidation Epithermal Deposit (PhD Thesis). University of Geneva, Terre et Environnement, p. 173.

Chambefort, I., Moritz, R., 2014. Subaqueous environment and volcanic evolution of the Late Cretaceous Chelopech Au–Cu epithermal deposit, Bulgaria. J. Volcanol. Geoth. Res. 289, 1–13.

Cruz, R., Bertrand, V., Monroy, M., Gonzalez, I., 2001. Effect of sulphide impurities on the reactivity of pyrite and pyritic concentrates: a multi-tool approach. Appl. Geochem. 16, 803–819.

Chopard, A., Benzaazoua, M., Plante, B., Bouzahzah, H., 2015. Kinetic tests to evaluate the relative oxidation rates of various sulfides and sulfosalts. In: Paper Presented at the 10th International Conference on Acid Rock Drainage & IMVA Annual Conference, Santiago, Chile.

Chopard, A., Plante, P., Benzaazoua, M., Bouzahzah, H., Marion, P., 2017. Geochemical investigation of the galvanic effects during oxidation of pyrite and base-metals sulfides. Chemosphere 166, 281–291.

Elghali, A., Benzaazoua, M., Bouzahzah, H., Bussiere, B., Villarraga-Gomez, H., 2018. Determination of the available acid-generating potential of waste rock, part I: mineralogical approach. Appl. Geochem. 99, 31–41.

Elghali, A., Benzaazoua, M., Bussiere, B., Bouzahzah, H., 2019. Determination of the available acid-generating potential of waste rock, part II: waste management involvement. Appl. Geochem. 100, 316–325.

Erguler, Z.A., Erguler, G., 2015. The effect of particle size on acid mine drainage generation: kinetic column tests. Miner. Eng. 76, 154–167. https://doi.org/10.1016/j.mineng.2014.10.002.

Fuerstenau, M.C., Chander, S., Woods, R., 2007. Sulfide mineral flotation. In: Fuerstenau, M.C., Jameson, G., Yoon, R. (Eds.), Froth Flotation - A Century of Innovation. Society for Mining, Metallurgy, and Exploration, Inc. (SME), Littleton, Colorado, pp. 425–464.

Georgieva, S., 2017. Mineral associations and their distribution in hydrothermal alteration zones of the Chelopech high-sulphidation deposit, Bulgaria. Geol. Balc. 46 (2), 11–16.

Georgieva, S., Velinova, N., Petrunov, R., Moritz, R., Chambefort, I., 2002. Aluminium phosphate– sulfate minerals in the Chelopech Cu–Au deposit: spatial development, chemistry and genetic significance. Mineral Petrol. Geochem. 39, 39–51.

Jambor, J.L., Dutrizac, J.E., Raudsepp, M., Groat, L.A., 2003. Effect of peroxide on neutralization-potential values of siderite and other carbonate minerals. J. Environ. Qual. 32, 2373–2378.

Kleinmann, R.L.P., Crerar, D.A., Pacellil, R.R., 1981. Biogeochemistry of acid mine drainage and a method to control acid formation. Min. Eng. 300–304.

Kwong, Y.T.J., 1993. Prediction and prevention of acid rock drainage from a geological and mineralogical perspective. In: MEND Report 1.32.1. CANMET, Ottawa.

Kwong, Y.T.J., Ferguson, K.D., 1997. Mineralogical changes during NP determinations and their implications. In: Proc. 4th Int. Conf. On Acid Rock Drainage, Vancouver, BC, Canada.

Lapakko, K.A., 1994. Evaluation of neutralization potential determinations for metal mine waste and a proposed alternative. In: Paper Presented at the Proceeding: of the Third International Conference on the Abatement of Acidic Drainage, April.

Lawrence, R.W., Wang, Y., 1997. Determination of neutralization potential in the prediction of acid rock drainage. In: Proc. 4th Int. Conf. On Acid Rock Drainage, Vancouver, BC, Canada.

Lawrence, R.W., Scheske, M., 1997. A method to calculate the neutralization potential of mining wastes. Environ. Geol. (Berl.) 32, 100–106.

Lindsay, M.B.J., Moncur, M.C., Bain, J.G., Jambor, J.L., Ptacek, C.J., Blowes, D.W., 2015. Review: geochemical and mineralogical aspects of sulfide mine tailings. Appl. Geochem. 57, 157–177.

Meek, F.A., 1981. Development of a procedure to accurately account for the presence of siderite during mining overburden analysis. In: 2nd Annual West Virginia Surface Mine Drainage Task Force Symposium, Virginia, USA.

Miller, S.D., Jeffery, J.J., Wong, J.W.C., 1991. Use and misuse of the acid-base account for AMD prediction. In: Blais (Ed.), 2ème Conférence Internationale sur la Réduction des Eaux de Drainage Acides. Nat. Resour. Canada, Montreal.

Morin, K.A., Hutt, N.M., 1994. Observed preferential depletion of neutralization potential over sulfide minerals in kinetic tests: site-specific criteria for safe NP/AP ratios. In: 3rd International Conference on the Abatement of Acidic Drainage. Pittsburg, USA, pp. 148–156.

Nicholson, R.V., Scharer, J.M., 1994. Laboratory studies of pyrrhotite oxidation kinetics. In: Alpers, C.N., Blowes, D.W. (Eds.), Environmental Geochemistry of Sulfide Oxidation, vol. 550. ACS Symposium Series, Washington, DC, pp. 14–30.

O'Connor, M., Olden, K., Overall, R., Meik, S., Kuzmanova, P., 2018. NI 43-101 Technical Report Mineral Resource & Reserve Update. United Kingdom.

Paktunc, A.D., 1999. Characterization of Mine Wastes for Prediction of Acid Mine Drainage Environmental Impacts of Mining Activities. Springer, pp. 19–40.

Parbhakar-Fox, A., Edraki, M., Bradshaw, D., Walters, S., 2009. Mineralogical characterisation techniques for predicting acid rock drainage. In: Enviromine 2009: First International Seminar on Environmental Issues in the Mining Industry, Santiago, Chile.

Parbhakar-Fox, A., Lottermoser, L.G., 2015. A critical review of acid rock drainage prediction methods and practices. Miner. Eng. 82, 107–124.

Perkin, E.H., Nesbitt, H.W., Gunter, W.D., St-Arnaud, L.C., Mycroft, J.R., 1995. Critical review of geochemical processes and geochemical models adaptable for prediction of acidic drainage from waste rock. In: MEND Report, Project 1.42.1.

Rincon, J., Gaydardzhiev, S., Stamenov, L., 2019. Coupling comminution indices and mineralogical features as an approach to a geometallurgical characterization of a copper ore. Miner. Eng. 130, 57–66.

Smith, K.S., Ramsey, C.A., Hageman, P.L., 2000. Sampling Strategy for the Rapid Screening of Mine-Waste Dumps on Abandoned Mine Lands. US Department of the Interior, US Geological Survey.

Sherlock, E.J., Lawrence, R.W., Poulin, R., et al., 1995. On the neutralization of acid rock drainage by carbonate and silicate minerals. Environ. Geol. 25, 43–54.

Skousen, J., Renton, J., Brown, H., Evans, P., Leavitt, B., Brady, K., Cohen, L., Ziemkiewicz, P., 1997. Neutralization potential of overburden samples containing siderite. J. Environ. Qual. 26, 673–681.

Sobek, A.A., Schuller, W.A., Freeman, J.R., 1978. Field and Laboratory Methods Applicable to Overburdens and Mine Soils Field and Laboratory Methods Applicable to Overburdens and Minesoils. EPA.

Stoykov, S., Yanev, Y., Moritz, R., Katona, I., 2002. Geological structure and petrology of the late cretaceous Chelopech volcano, Srednogorie magmatic zone. Mineral Petrol. Geochem. 39, 27–38.

Todorova, E., Avramov, I., Georgakiev, I., 2017. Technology for backfilling of mined-out areas with paste fill applied at Dundee Precious Metals Chelopech. J. Min. Geol. Sci. 60, 10–16.

Villeneuve, M., Bussiere, B., Benzaazoua, M., Aubertin, M., Monroy, M., 2003. The influence of kinetic test type on the geochemical response of low acid generating potential tailings. In: Proceedings of Tailings and Mine Waste '03, Sweets and Zeitlinger. Vail, CO, USA.

Weber, P.A., Thomas, J.E., Skinner, W.M., Smart, R.StC., 2004. Improved acid neutralisation capacity assessment of iron carbonates by titration and theoretical calculation. Appl. Geochem. 19, 687–694.

Wills, B.A., Finch, J.A., 2016. Froth flotation. In: Wills, A.B., Finch, J.A. (Eds.), Wills' Mineral Processing Technology, an Introduction to the Practical Aspects of Ore Treatment and Mineral Recovery. Butterworth-Heinemann, Boston, pp. 265–380.

Zhang, Q., Xu, Z., Bozkurt, V., Finch, J., 1997. Pyrite flotation in the presence of metal ions and sphalerite. Int. J. Miner. Process. 52, 187–201.